Research Square

Preprints are preliminary reports that have not undergone peer review.
They should not be considered conclusive, used to inform clinical practice,
or referenced by the media as validated information.

Plastic-associated freshwater bacteria promote microplastic aggregation, alter trophic transfer, and serve as chassis for engineered plastic modification

José Ramón López
Universidade de Santiago de Compostela
Sergio Silva-Bea
Universidade de Santiago de Compostela
Maxim Tiburziano
Universidade de Santiago de Compostela
José Llovo
Universidade de Santiago de Compostela
Juan José Nieto-Fontarigo
Universidade de Santiago de Compostela
Ana Otero
Universidade de Santiago de Compostela
Manuel Romero
manuelromero.bernardez@usc.es

Universidade de Santiago de Compostela

Article

Keywords: Microplastic aggregation, Plastisphere, Extracellular polymeric substances, Biofilms, Trophic transfer, Freshwater ecosystems

Posted Date: November 20th, 2026

DOI: https://doi.org/10.21203/rs.3.rs-10988715/v1

License: This work is licensed under a Creative Commons Attribution 4.0 International License.
Read Full License

Additional Declarations: No competing interests reported.

Plastic-associated freshwater bacteria promote microplastic aggregation, alter trophic transfer, and serve as chassis for engineered plastic modification

José Ramón López[1,2], Sergio Silva-Bea[1,2], Maxim Tiburziano[3], José Llovo[1,2], Juan José Nieto-Fontarigo[2,4,5], Ana Otero[1,2], Manuel Romero[1,2]*

[1]Department of Microbiology, Faculty of Biology, Universidade de Santiago de Compostela, 15782 Santiago de Compostela, Spain

[2]Aquatic One Health Research Center (iARCUS), Universidade de Santiago de Compostela, 15782 Santiago de Compostela, Spain

[3]Department of Physical Chemistry, Biological Chemistry and Molecular Materials Research Center (CIQUS), Universidade de Santiago de Compostela, 15782 Santiago de Compostela, Spain

[4]Department of Biochemistry and Molecular Biology, Faculty of Biology, Universidade de Santiago de Compostela, 15782 Santiago de Compostela, Spain

[5]Translational Research in Airway Diseases Group (TRIAD), Health Research Institute of Santiago de Compostela (IDIS), Santiago de Compostela, Spain

* Correspondence to Manuel Romero: manuelromero.bernardez@usc.es

Abstract

Environmental plastic debris harbors distinct microbial communities, yet the functional traits associated with plastisphere colonization remain poorly understood. Here, we isolated 230 bacterial strains from riverine plastic debris and surrounding freshwater samples and screened their ability to aggregate fluorescent polystyrene microplastics (MPs). Plastic-associated isolates displayed significantly stronger aggregation phenotypes than water-derived bacteria, with multiple environmental strains removing more than 95% of suspended MPs. Comparative analyses revealed that highly aggregative isolates differed markedly from their corresponding type strains and possessed diversified extracellular polysaccharide biosynthetic repertoires. Aggregation dynamics were strongly influenced by hydrodynamic conditions and bacterial abundance, while theoretical encounter-rate analyses indicated that incomplete MP removal was constrained primarily by attachment efficiency, aggregate architecture, and sedimentation behavior rather than by particle encounter frequency. Highly aggregative strains consistently reduced MP availability to suspension-feeding rotifers, whereas effects on phagocytic amoebae were more limited, indicating grazer-dependent impacts on trophic transfer. To explore whether MP-capturing bacteria can be repurposed as platforms for plastic-interacting functions, the

highly aggregative isolate *Pseudomonas parakoreensis* A16 was engineered to express FastPETase, resulting in detectable alterations of PET surface chemistry. These findings suggest that plastisphere-associated bacteria are enriched in traits promoting MP sequestration and may serve as versatile chassis coupling particle capture with engineered plastic-modifying functions. Together, our results identify bacterial aggregation as a central process linking microbial colonization, microplastic fate, and trophic transfer in freshwater ecosystems.

Keywords

Microplastic aggregation; Plastisphere; Extracellular polymeric substances; Biofilms; Trophic transfer; Freshwater ecosystems

Introduction

The widespread accumulation of microplastics (MPs) in aquatic environments has emerged as a global environmental concern. MPs are now routinely detected in freshwater, estuarine, and marine ecosystems, where they can remain suspended for extended periods, undergo long-range transport, and interact with diverse biological communities (Wang et al., 2021; Zhang et al., 2024). Their small size facilitates uptake by a wide range of organisms, including protozoa, zooplankton, invertebrates, and vertebrates, raising concerns regarding trophic transfer and ecosystem-level impacts (Botterell et al., 2020; Gouin, 2020).

Upon entering aquatic systems, plastic particles rapidly become colonized by microorganisms, giving rise to biofilm-covered habitats collectively referred to as the plastisphere (Zettler et al., 2013). Plastisphere communities often differ markedly from the surrounding planktonic microbiota and are frequently enriched in taxa associated with surface colonization, biofilm formation, and particle-attached lifestyles (Bryant et al., 2016; Miao et al., 2021; Wright et al., 2020; Song et al., 2024). These observations have stimulated considerable interest in understanding the ecological and functional significance of plastic-associated microbial assemblages. However, most studies have focused on community composition, succession dynamics, and taxonomic diversity, whereas the ecological functions that may be selected on plastic surfaces remain comparatively poorly understood (Wang et al., 2021; Cholewińska et al., 2025).

One process that may be particularly important is MP aggregation. In aquatic environments, aggregation influences particle transport, vertical fluxes, residence times, and biological availability. Interactions between MPs and biogenic particles can lead to the formation of larger aggregates whose physical properties

determine whether particles remain suspended or are transferred to sediments (Long et al., 2015; Kooi et al., 2017). Microbial biofilms and extracellular polymeric substances (EPS) are increasingly recognized as important drivers of these processes. EPS can enhance particle adhesion, alter aggregate architecture, and regulate settling behavior, playing a central role in the formation of marine snow and other suspended particulate assemblages (Passow, 2002; Burd and Jackson, 2009; Quigg et al., 2021). Recent studies have also shown that microbial colonization can substantially modify the aggregation and sinking dynamics of MPs (Michels et al., 2018; Nguyen et al., 2020).

Despite growing recognition of the importance of microbial-mediated aggregation, relatively little is known about the extent to which aggregation represents a strain-specific microbial trait or whether plastic-associated environments are enriched in bacteria with enhanced MP-capturing capacity. Most previous work has focused on model organisms or mixed microbial communities, leaving unresolved whether environmental plastisphere bacteria possess specialized traits that promote particle capture and sequestration. Similarly, the contribution of specific extracellular matrix components and the ecological consequences of bacterial aggregation for MP bioavailability and trophic transfer remain poorly characterized.

Previously, we demonstrated that the opportunistic pathogen *Pseudomonas aeruginosa* PAO1 can capture, aggregate, and sediment polystyrene MPs through mechanisms involving the cell-associated Psl exopolysaccharide and fluid-mediated particle encounters (Romero et al., 2022). Whether similar or even more efficient aggregation phenotypes occur among environmental bacteria naturally associated with plastic debris remains unknown. Addressing this question is essential for understanding how microbial colonization influences the environmental fate of MPs in natural ecosystems.

Here, we isolated 230 bacterial strains from plastic debris and surrounding waters of a freshwater river system and screened their capacity to aggregate MPs. We show that plastic-associated bacteria are strongly enriched in MP-capturing phenotypes and that highly aggregative environmental isolates possess diversified EPS-associated biosynthetic repertoires compared with their corresponding type strains. We further demonstrate that MP aggregation is shaped by hydrodynamic conditions and bacterial abundance, that aggregation modifies MP trophic transfer to aquatic grazers in a feeding-mode-dependent manner, and that the highly aggregative isolate *Pseudomonas parakoreensis* A16 can be engineered as a chassis for PET surface modification through heterologous expression of FastPETase. Together, these findings identify bacterial aggregation as a key process linking plastisphere colonization, MP fate, and biological interactions in freshwater environments.

Materials and methods

1. Sampling, bacterial isolation and culture conditions

Plastic-associated bacterial isolates were recovered from the Sar River (Galicia, NW Spain) during a single sampling campaign conducted in December 2024. A total of eight independent plastic-associated samples (A, C, L, P, D, G, K and T) were collected from two freshwater river locations situated upstream and downstream of a wastewater treatment plant (WWTP) discharge point. Sampling sites included an upstream location (42.871916°N, 8.585170°W) and a downstream location (42.868778°N, 8.600512°W). For comparative purposes, surrounding water samples were collected in parallel from the same locations.

To isolate biofilm-associated bacteria, plastic fragments were first rinsed gently with sterile phosphate-buffered saline (PBS) to remove loosely attached debris. The samples were then transferred to sterile PBS, vortexed, and sonicated in a water bath (Branson 8510) for 10 min at 40 kHz to detach the sessile microbial community. Tenfold serial dilutions in PBS were plated onto Tryptic Soy Agar (TSA) and incubated at 25 °C. Representative colonies showing distinct macromorphologies were picked, purified through successive streaking, and stored at −80 ºC in Tryptic Soy Broth (TSB) supplemented with 30% (v/v) glycerol. Routine cultivation of the isolates was performed in Lysogeny Broth (LB) at 25 ºC under shaking conditions (150 rpm), unless otherwise specified.

2. Identification, whole-genome sequencing and comparative genomic analyses

Preliminary taxonomic identification of isolates was performed by partial 16S rRNA gene sequencing. Genomic DNA was obtained from overnight cultures using a boiling extraction procedure consisting of incubation in distilled water for 5 min followed by centrifugation at 16,000 x g for 2 min. Amplification of the 16S rRNA gene was performed according to Weisburg et al. (1991) using DreamTaq PCR Master Mix (Thermo Scientific). PCR products were purified using the QIAquick PCR & Gel Cleanup Kit (Qiagen) and sequenced by STABvida (Lisbon, Portugal). Taxonomic assignments were obtained using the EzBioCloud database.

Selected isolates displaying strong MP aggregation phenotypes were further characterized by whole-genome sequencing (WGS). Genomic DNA was extracted using the QIAsymphony DSP Virus/Pathogen Midi Kit (Qiagen, Hilden, Germany) and quantified using the Qubit dsDNA HS Assay Kit (Thermo Fisher Scientific). Libraries were prepared using the Illumina DNA Prep kit (Illumina, San Diego, USA) and sequenced on an Illumina MiSeq platform using MiSeq Reagent Kit v3 chemistry (2 × 300 bp paired-end reads).

Raw reads were quality-filtered and assembled de novo using SPAdes. Preliminary species identification was performed using Mash distance comparisons against publicly available genomes. Species assignments were subsequently confirmed by Average Nucleotide Identity (ANI) analyses using FastANI. ANI values above 95% were considered indicative of the same species.

Extracellular polysaccharide (EPS)-associated operons were identified using EPSsmash (Daugberg et al., 2025). Comparative synteny analyses between environmental isolates and reference genomes were performed using CAGECAT (van den Belt et al., 2023).

3. MP aggregation screening assays

MP aggregation assays were performed using fluorescent polystyrene microspheres (Fluoro-Max Green, Thermo Scientific) with a nominal diameter of 0.5 µm. MPs were suspended at a final concentration of 1×10^8 particles mL^{-1} in sterile distilled water. Bacterial suspensions were adjusted to a final OD600 of 0.01 in a total assay volume of 8 mL. Based on representative cell counts obtained for selected isolates, this optical density corresponded approximately to 10^7 cells mL^{-1}.

Samples were incubated at room temperature in sealed glass vials (approximately 9 mL total capacity) containing 8 mL of suspension. Vials were mounted horizontally on a roller mixer operating at 33 rpm to maintain particles in suspension and promote particle-cell encounters while minimizing sedimentation. Unless otherwise indicated, incubations were performed for 24 h.

Following incubation, samples were allowed to stand for 45 min to facilitate sedimentation of large aggregates. Aliquots (100 µL) were carefully collected from the upper phase of each vial, and fluorescence corresponding to suspended MPs was quantified using a Spark microplate reader (TECAN) with excitation/emission settings appropriate for green fluorescent microspheres (Firefli™ 468/508nm). MP concentrations were estimated from calibration curves relating fluorescence intensity to particle concentration. This assay provides an operational measure of MPs remaining in suspension after incubation and sedimentation, integrating the combined effects of aggregation, settling, and particle retention within the experimental system.

Pseudomonas aeruginosa PAO1, previously shown to promote EPS-dependent MP aggregation, was included as a reference strain in all assays. Abiotic controls containing MPs without bacteria were included in parallel.

4. Effect of hydrodynamic conditions, incubation time and bacterial concentration on MP aggregation

To evaluate the influence of environmental and experimental parameters on MP aggregation dynamics, selected isolates were tested under different incubation regimes.

For hydrodynamic comparisons, aggregation assays were performed either under rolling incubation or under static conditions. Incubation times of 24 h and 48 h were evaluated for each condition.

To assess the effect of bacterial abundance, assays were performed using a 10-fold serial dilution series spanning six initial bacterial concentrations. The highest concentration corresponded to approximately 10^8 cells mL^{-1} (equivalent to an OD600 of 0.1 under the conditions used), and each subsequent condition represented a 10-fold dilution.

To evaluate potential cooperative interactions, pairwise and three-strain mixtures were prepared while maintaining a total bacterial concentration equivalent to that used in the screening assays (final OD600 = 0.01). Mixed cultures were evaluated under both rolling and static conditions after 24 h and 48 h of incubation.

In all experiments, suspended MPs remaining after incubation were quantified as described above.

5. Estimation of diffusion coefficients and encounter rates

Diffusion coefficients for MPs and bacterial cells were estimated using the Stokes–Einstein equation:

$$D = \frac{k_B T}{6\pi\mu r}$$

where k_B is the Boltzmann constant, T the absolute temperature (293 K), μ the dynamic viscosity of water at 20 °C, and r the particle radius. MPs were assumed to have a diameter of 0.5 µm, while bacterial cells were approximated as spherical particles with a diameter of 1 µm.

Diffusion-driven encounter rates between MPs and bacterial cells were estimated using the classical Smoluchowski heteroaggregation kernel:

$$\Gamma_{diff} = 4\pi(D_A + D_B)(r_A + r_B)$$

where D_A and D_B are the diffusion coefficients and r_A and r_B the radii of MPs and bacterial cells, respectively.

Encounter frequencies per unit volume were calculated as:

$$R = \Gamma_{diff} C_A C_B$$

where C_A and C_B denote MP and bacterial concentrations in suspension.

To qualitatively relate theoretical diffusion-limited encounter rates to experimentally observed aggregation dynamics, an effective collision efficiency parameter (α) was introduced:

$$\Gamma_{eff} = \alpha\, \Gamma_{diff}$$

An approximate aggregation timescale was then estimated as:

$$\tau \sim \frac{1}{\alpha\, \Gamma_{diff}\, C}$$

where C represents the relevant particle concentration governing encounter frequency.

No direct estimation of the collision efficiency (α) was performed. Instead, this parameter is used as a conceptual descriptor accounting for deviations from ideal diffusion-limited aggregation ($\alpha = 1$), including physicochemical constraints on particle attachment, as well as downstream processes such as aggregate restructuring, sedimentation, and persistence in suspension. This framework was used to interpret aggregation dynamics and identify potential constraints beyond diffusion-limited encounters.

6. Amoeba uptake assays

The freshwater environmental amoeba isolate *Acanthamoeba* sp. H13 was used to evaluate the influence of bacterial aggregation on MP uptake by phagocytic grazers. Three bacterial strains displaying distinct aggregation phenotypes were selected: the highly aggregative isolate *Pseudomonas parakoreensis* A16, *Pseudomonas aeruginosa* PAO1, and the PAO1 Δ*psl* mutant deficient in Psl exopolysaccharide production.

Amoebae were maintained in PYG medium and routinely propagated using heat-killed *Escherichia coli* DH5α cells as a food source at 30 °C. Amoeba inocula were prepared by centrifugation at 200 × g for 10 min followed by resuspension in sterile distilled water. Cell concentrations were determined using a Neubauer counting chamber.

MP-bacteria mixtures were prepared as described for aggregation assays and incubated under rolling conditions for 24 h prior to amoeba addition. Amoebae were subsequently added to obtain a final concentration of 2,250 trophozoites mL^{-1} and incubated for an additional 48 h under rolling conditions to allow phagocytosis of MP-bacteria aggregates. Control treatments included: MPs without bacteria, MPs plus bacteria without amoebae, and amoebae incubated without MPs.

At the end of the incubation period, samples were passed through 80 µm mesh filters to remove large aggregates that could interfere with flow-cytometric analysis. This filtration step was intended to exclude oversized aggregates while preserving the amoebal fraction for subsequent analysis. Filtered samples were then analyzed using a CytoFLEX flow cytometer (Beckman Coulter) equipped with a B3-R2-V2 optical configuration. Fluorescent MPs were excited using the 488 nm blue laser and fluorescence emission was collected through the FITC channel (525/40 nm band-pass filter). Instrument performance was routinely verified using fluorescent calibration beads (CytoFlex daily QC fluorospheres) according to the manufacturer's recommendations. Samples were acquired for 4 min at constant instrument settings and flow rates to ensure comparable sampling volumes across treatments.

Amoebae were initially identified based on their forward and side scatter (FSC-A/SSC-A) characteristics, while MPs were discriminated using their green fluorescence signal. Gates were established using control samples containing only amoebae, only MPs, only bacteria, and MPs-bacteria mixtures without amoebae. Internalization of MPs was estimated as the percentage of amoebae displaying fluorescence above the threshold established from amoeba-only controls. Median fluorescence intensity (MFI) within the amoebae population was used as an indirect measure of the relative amount of internalized MPs per amoeba. Data were analyzed using CytExpert v2.6 software, and statistical analysis was performed with GraphPad Prism version 10 software.

Microscopy observations were performed using an Eclipse E400 microscope (Nikon) equipped with a Nikon B-2A fluorescence filter cube (BP450–490, DM505, BA520). Fluorescent MPs were visualized by epifluorescence microscopy while simultaneously observing amoebae using phase-contrast optics. Suspended MP concentrations were monitored throughout the assay as described for aggregation experiments.

Experiments were performed in three independent biological replicates with duplicate technical replicates per experiment.

7. Rotifer uptake assays

The rotifer *Brachionus plicatilis* was used to evaluate the influence of bacterial aggregation on MP uptake by suspension-feeding grazers. Rotifers were maintained in aerated seawater cultures at 25 °C and fed microalgae (*Tetraselmis chuii* and *Chlorella* sp.). Before the experiments, rotifers were transferred to food-free seawater for 24 h. Rotifer inocula were prepared by filtration through 40 µm mesh filters followed by resuspension in sterile seawater. Rotifer concentrations were determined microscopically using Lugol-fixed samples. Bacterial strains

used in the assays were confirmed to be capable of growth under marine conditions by cultivation on Marine Agar and TSA prepared with seawater.

MP-bacteria mixtures were generated as described for aggregation assays except that sterile seawater was used instead of distilled water. Following 24 h of rolling incubation, rotifers were added to obtain a final concentration of 500 rotifers mL^{-1} and samples were analyzed after 3 h and 24 h of exposure under rolling conditions. At the end of the incubation period, samples were filtered through 40 µm mesh filters to recover rotifers. Retained organisms were washed with sterile seawater and resuspended for fluorescence quantification using the TECAN Spark microplate reader. Additional aliquots were fixed with Lugol solution and examined microscopically using fluorescence microscopy. Suspended MP concentrations were quantified throughout the assay as described above.

Experiments were performed in three independent biological replicates with three technical replicates per experiment.

8. Construction of FastPETase-expressing strains

The FastPETase coding sequence (Lu et al., 2022) was synthesized and cloned into pBluescript II KS(+) by GenScript (Piscataway, NJ, USA). Plasmid DNA was propagated in *Escherichia coli* DH5α and purified using a QIAprep Spin Miniprep Kit (Qiagen). The FastPETase insert and the pME6032 expression vector were digested with EcoRI and BglII, purified from agarose gels, and ligated using T4 DNA ligase (Thermo Fisher Scientific). The resulting pME6032-FastPETase construct was transformed into *E. coli* DH5α, recovered from tetracycline-resistant clones, and subsequently introduced into *P. parakoreensis* A16 and *P. aeruginosa* PAO1 by electroporation. Recombinant strains were selected on tetracycline-containing LB agar (125 µg mL^{-1}) and verified by PCR and Sanger sequencing.

9. PET incubation assays and ATR-FTIR analyses

To evaluate PET surface modification, bacterial strains were incubated with PET films (Mylar PET film, 23 µm thickness). Assays were performed in 6-well polystyrene plates containing 5 mL of liquid carbon-free basal medium (LCFBM) (Kim et al., 2020) supplemented with tetracycline where appropriate. Initial bacterial concentrations corresponded to OD600 = 0.01. Incubations were performed statically at 25 °C. The following strains were included: A16 + pME6032-FastPETase, PAO1 + pME6032-FastPETase, parental A16, parental PAO1 and bacteria-free controls.

PET films were recovered after 18 days of incubation and subjected to a cleaning procedure adapted from Miravalle et al. (2024) to remove attached biomass and extracellular material prior to spectroscopic analysis. Briefly, films were sequentially washed with Milli-Q water, subjected to repeated sonication steps,

treated with 5% sodium dodecyl sulfate (SDS), extensively rinsed with Milli-Q water, and vacuum-dried before analysis. This protocol was previously developed and validated to remove biological material from plastic surfaces while preserving polymer integrity for attenuated total reflectance Fourier-transform infrared spectroscopy (ATR-FTIR) characterization.

For each PET film, ATR-FTIR spectra were acquired at five independent surface positions (four peripheral regions and the centre) to account for spatial heterogeneity. Spectra were recorded using a PerkinElmer Spectrum Two ATR-FTIR spectrometer equipped with a diamond ATR accessory at a resolution of 4 cm^{-1} with eight co-added scans per measurement. Spectra showing acquisition artifacts were excluded from further analysis.

Diagnostic PET spectral bands located at 1340 and 1370 cm^{-1} were selected for targeted analysis based on their reported association with polymer morphology and crystallinity (Chen et al., 2012). Spectra were baseline-corrected and normalized prior to comparison. The integrated areas of the 1340 and 1370 cm^{-1} bands were calculated and the 1340/1370 peak-area ratio was used as a comparative indicator of changes in PET spectral properties.

Additional FTIR analyses were performed using polystyrene substrates incubated with selected environmental isolates to evaluate potential evidence of polymer degradation.

10. Statistical analyses

Statistical analyses were performed using GraphPad Prism version 10 (GraphPad Software, Boston, MA, USA). Data are presented as mean ± standard deviation (SD) unless otherwise indicated. Data distributions were assessed using the Shapiro-Wilk test. Comparisons between plastic-associated and water-derived isolates were performed using the Mann-Whitney test because the aggregation screening dataset did not satisfy the assumptions of normality.

Experiments evaluating the effects of incubation regime, incubation time, bacterial concentration, and strain combinations on MP aggregation were analyzed using ordinary two-way analysis of variance (ANOVA) followed by Bonferroni's multiple-comparisons test. Comparisons among multiple treatments in amoeba and rotifer uptake assays were performed using one-way ANOVA followed by Tukey's multiple-comparisons test.

Results and discussion

1. Environmental plastic-associated bacteria are enriched in MP-capturing phenotypes

Plastic debris provides a unique surface-associated habitat that may select for bacterial traits promoting particle attachment and retention. To evaluate whether plastic-associated environments are enriched in bacteria with enhanced MP-capturing capacity, a total of 230 isolates were recovered from the Sar River, including 184 isolates recovered from eight plastic-associated samples and 46 isolates recovered from surrounding water samples. Seven plastic-associated samples originated from the upstream location (samples C, D, G, K, L, P and T), yielding 24, 22, 23, 19, 25, 24 and 23 isolates, respectively (160 isolates in total). A single plastic-associated sample was collected downstream of the wastewater treatment plant (sample A), from which 24 isolates were recovered.

The MP aggregation capacity of all isolates was evaluated using a suspension assay containing 10^8 fluorescent polystyrene MPs mL^{-1}. *Pseudomonas aeruginosa* PAO1 was included as a reference strain because of its previously characterized MP aggregation phenotype (Romero et al., 2022). After 24 h under rolling incubation, PAO1 reduced suspended MPs to 9.2×10^6 MPs mL^{-1}, corresponding to a 90.8% reduction relative to the particle-only control. Notably, nine environmental isolates displayed aggregation capacities equal to or greater than PAO1 (**Figure 1A; Table 1**). These isolates belonged predominantly to the genera *Pseudomonas* (55%) and *Acinetobacter* (22%), together with representatives of *Deinococcus* and *Bacillus*. Remarkably, four of the nine high-performing isolates (44%) originated from sample A, indicating that the downstream plastic-associated sample was enriched in bacteria displaying strong MP aggregation phenotypes.

Among all isolates, strain A16 (*Pseudomonas parakoreensis*) exhibited the strongest phenotype, reducing suspended MPs by 97.9% and reaching residual concentrations close to 10^6 MPs mL^{-1}. Similarly, *Deinococcus aquaticus* P5 and *Acinetobacter johnsonii* A20 showed reductions of 97.1% and 94.2%, respectively. In contrast, isolates from surrounding water samples generally displayed significantly lower aggregation capacity than plastic-associated isolates (**Figure 1B**), supporting the hypothesis that plastic-associated environments are correlated with an increased frequency of bacterial traits promoting MP attachment and aggregation. Although aggregation phenotypes were generally reproducible across replicates, some isolates exhibited greater variability in residual MP concentrations than others (**Table 1**), suggesting that aggregate formation and sedimentation may be intrinsically more heterogeneous in certain strains.

This enrichment is consistent with previous studies showing that plastic debris in aquatic environments supports distinct microbial communities, often enriched in surface-associated and biofilm-forming taxa compared to the surrounding water (Miao et al., 2021; Wright et al., 2020; Zettler et al., 2013; Song et al., 2024;

Cholewińska et al., 2025). Plastic surfaces may therefore act not only as substrates for colonization but also as ecological filters selecting for traits such as adhesion, extracellular matrix production, and particle-associated lifestyles.

To assess whether this phenotype reflects species-level traits or isolate-specific adaptations, three high-performing isolates (A16, P5, and A20) were compared with their corresponding type strains. Whole-genome sequencing confirmed species assignments and guided selection of reference genomes. While environmental isolates reduced MPs by 94.2-97.9%, the corresponding type strains showed little or no aggregation activity (0-13% reduction; **Table 1**). These findings indicate that strong MP aggregation is not a conserved species trait but is instead associated with environmental strains from plastic debris, likely reflecting strain-level adaptation to plastic-associated habitats. This interpretation aligns with previous work showing that plastic debris hosts microbial communities distinct from planktonic populations (Bryant et al., 2016; Song et al., 2024).

Given our previous finding that the Psl exopolysaccharide contributes to MP aggregation in *P. aeruginosa* PAO1, we next examined whether highly aggregative environmental isolates possess distinctive EPS biosynthetic repertoires. EPS operons were identified using EPSsmash (Daugberg et al., 2025) and compared with homologous loci from reference genomes by synteny analysis using CAGECAT (van den Belt et al., 2023) (**Supplementary Figure S1**). All three environmental isolates encoded multiple Wzy-dependent EPS clusters, commonly involved in the synthesis of structurally complex extracellular polysaccharides associated with adhesion, biofilm architecture, and surface interactions (Islam and Lam, 2014), suggesting a potential role in MP capture.

Specifically, *P. parakoreensis* A16 contained four EPS-associated operons, including two Wzy-dependent loci and an additional PNAG-*pga* operon absent from the reference genome. Comparative analysis showed overall conservation of Wzy-dependent loci, although one operon displayed evidence of local structural rearrangement. Similarly, *A. johnsonii* A20 encoded a Wzy-dependent operon together with a PNAG-*pga* locus not detected in the reference strain, alongside substantial reorganization of the Wzy-dependent region. In contrast, *D. aquaticus* P5 exhibited the most divergent repertoire, with three distinct Wzy-dependent operons that did not closely match the single locus identified in the reference genome. Instead, homologous operons were found in other *Deinococcus* species, suggesting diversification or acquisition of EPS biosynthetic loci in environmental populations.

Although these analyses do not establish a direct causal role for specific polysaccharides in MP capture, the recurrent expansion and diversification of Wzy-dependent and PNAG-associated EPS systems among high-performing isolates

suggest that variation in extracellular matrix biosynthetic capacity may contribute to enhanced MP aggregation. However, MP aggregation is influenced by multiple factors, including polymer physicochemistry, conditioning films, hydrodynamic conditions, and stochastic community assembly processes, indicating that EPS composition alone is unlikely to fully explain plastisphere selection dynamics (Wang et al., 2021; Zhang et al., 2024).

Collectively, these results indicate that plastic-associated freshwater bacteria are enriched in phenotypes promoting MP aggregation and sequestration. While previous studies have shown that plastisphere communities are taxonomically distinct and enriched in biofilm-forming taxa such as *Pseudomonas* and *Acinetobacter* (Cholewińska et al., 2025), our findings extend this view by demonstrating that these communities are also enriched in functional traits linked to particle capture. The markedly higher aggregation capacities of environmental isolates compared to their corresponding type strains further support the idea that plastic-associated habitats select for bacterial variants with enhanced surface-interaction capabilities, potentially facilitating stable colonization of suspended plastic substrates in aquatic environments (Song et al., 2024).

2. MP aggregation dynamics are shaped by hydrodynamic conditions and bacterial abundance

The influence of hydrodynamic conditions and incubation time on MP aggregation was next evaluated using the selected high-performing isolates. Overall, most strains displayed substantially greater MP removal under rolling incubation than under static conditions (**Figure 2A**), consistent with the established role of fluid motion in enhancing particle encounters and aggregate formation in aquatic systems (Romero et al., 2022; Long et al., 2015; Kooi et al., 2017).

Isolates A16, A20, and P5 all produced significantly greater reductions in suspended MPs under rolling conditions at both 24 h and 48 h compared to static incubation. The strongest effect was observed for *D. aquaticus* P5, for which the number of suspended MPs after 24 h was approximately one order of magnitude higher under static conditions than under rolling incubation. In comparison, the differences between static and rolling conditions were approximately 3-4 fold for A16 and 2-3 fold for A20. In contrast, *P. aeruginosa* PAO1 showed comparatively limited sensitivity to hydrodynamic conditions.

These observations are in agreement with general models of aquatic particle aggregation in which Brownian motion, shear-driven transport, and differential particle movement increase the probability of particle-cell encounters (Kooi et al., 2017). In such systems, EPS contribute to aggregation by mediating particle

adhesion and promoting the formation of cohesive suspended matrices (Passow, 2002; Long et al., 2015). The stronger dependence of environmental isolates on rolling conditions compared to PAO1 further suggests that strain-specific properties, including surface adhesion characteristics, EPS production, and aggregate architecture, influence MP capture efficiency under dynamic conditions.

Incubation time also affected MP removal dynamics, although the magnitude of this effect depended on both strain identity and hydrodynamic regime. Under static conditions, all strains showed significant reductions in suspended MPs between 24 h and 48 h, indicating continued aggregation and/or sedimentation over time. However, the magnitude of this reduction varied substantially between isolates, ranging from a 66% decrease for A16 to only 33% for P5. Under rolling conditions, by contrast, MP removal approached saturation more rapidly. No significant differences between 24 h and 48 h were observed for A16 or PAO1, whereas A20 and P5 showed modest additional MP reductions at 48 h. These results suggest that hydrodynamic mixing accelerates aggregation kinetics and rapidly reduces the pool of freely suspended particles available for further encounters.

To further investigate the relationship between bacterial abundance and aggregate formation, the effect of inoculum concentration on MP removal was evaluated using a 10-fold concentration series spanning six bacterial doses (**Figure 2B**). As expected, increasing bacterial concentrations generally promoted greater reductions in suspended MPs, consistent with higher probabilities of particle-cell encounters and enhanced EPS-mediated aggregation. However, this trend did not scale linearly at the highest bacterial concentrations tested. Notably, for isolates A16, A20, and P5, the maximum reduction in suspended MPs was not observed at the highest bacterial dose (10^8 cells mL^{-1}), but rather at the intermediate dose corresponding to the concentration originally used during screening (10^7 cells mL^{-1}).

This non-linear response suggests that increasing bacterial abundance alone is insufficient to continuously improve MP capture. One plausible explanation is that elevated cell densities alter EPS production dynamics and aggregate microstructure, thereby affecting particle accessibility, aggregate porosity, and collision efficiency. Similar non-linear relationships between microbial density, extracellular matrix architecture, and aggregation behavior have been described in natural aquatic particle systems (Passow, 2002; Kiørboe, 2003).

Finally, the potential for cooperative interactions between strains was assessed by combining isolates in pairwise or three-strain mixtures under four incubation conditions (rolling/static; 24 h/48 h), while maintaining a total bacterial concentration comparable to that used during screening (**Figure 2C**). In most

cases, mixed cultures did not improve MP removal beyond that achieved by the most efficient isolate present in the consortium, suggesting limited synergistic interactions during aggregate formation. One notable exception was the combination of isolates A20 and P5, which showed a significantly greater reduction in suspended MPs under rolling conditions compared with either strain alone.

This enhanced performance suggests that specific combinations of environmental isolates may exhibit complementary aggregation-related traits. Such effects could arise from differences in EPS composition, surface properties, or particle-binding affinities that collectively improve aggregate stability and MP incorporation. However, the generally limited improvement observed in mixed cultures indicates that MP capture is predominantly governed by dominant strain-specific traits rather than additive community effects. Nevertheless, the observed synergy in the A20+P5 consortium highlights that cooperative interactions can emerge under specific hydrodynamic and compositional conditions, potentially contributing to MP aggregation processes in natural multispecies biofilms and suspended particle assemblages.

Despite the strong influence of hydrodynamic conditions and bacterial abundance on aggregation performance, even the most efficient isolates consistently left residual suspended MP concentrations in the range of 10^6-10^7 MPs mL^{-1} after 24 h, corresponding to approximately 2-10% of the initial particle load. This observation suggests that factors beyond simple encounter frequency contribute to the ultimate limits of MP removal.

3. Selected isolates promote rapid aggregation but incomplete removal from suspension

To better understand why even the most efficient isolates did not completely remove MPs from suspension, we next examined the physical constraints governing MP-bacteria encounters and aggregate formation. Diffusion-driven encounter rates between MPs (0.5 µm diameter) and bacterial cells (1 µm diameter) were estimated using the Stokes-Einstein relation together with classical Smoluchowski heteroaggregation theory, which provides a fundamental framework for describing collision dynamics in colloidal and aquatic particle systems (Smoluchowski, 1917; Burd and Jackson, 2009).

At 20 ºC in water, the resulting diffusion-limited aggregation kernel is on the order of 10^{-17} m^3 s^{-1}. At the initial concentrations used in the aggregation assays (10^8 MPs mL^{-1} and approximately 10^7 bacterial cells mL^{-1}), this corresponds to a theoretical encounter frequency on the order of 10^4 particle-cell encounters mL^{-1} s^{-}

^{1}, indicating that particle-cell contacts are not rate-limiting under the conditions tested. Using these parameters, the characteristic timescale associated with diffusion-driven encounters is on the order of 3 h. These calculations should be interpreted as lower-bound estimates because they consider only Brownian diffusion-driven encounters. Under the rolling conditions used in the experiments, fluid motion, particle transport, and shear-induced collisions are also expected to contribute to encounter frequencies, thereby increasing the probability of particle-cell interactions beyond that predicted by diffusion alone.

To further contextualize the aggregation dynamics predicted by Smoluchowski theory, previously published laser-diffraction datasets from PAO1-mediated MP aggregation (Romero et al., 2022) were reanalyzed (**Supplementary Figure S2**). This analysis revealed a rapid redistribution of particle-size classes during the first hours of incubation, characterized by a progressive shift from submicron particles toward particle populations centered around 10-20 µm. Most of this redistribution occurred within the first 3-5 h, after which particle-size distributions changed only modestly, indicating the approach to a quasi-steady state. Aggregate formation was detectable within the first hour of incubation, demonstrating that particle encounters occur rapidly, whereas subsequent processes such as aggregate growth, restructuring, and sedimentation govern the overall evolution of the system. Similar aggregation kinetics have been described in marine particle systems, where EPS and transparent exopolymer particles (TEP) facilitate rapid formation of cohesive aggregates following particle encounter (Passow, 2002; Burd and Jackson, 2009).

Although encounter frequencies are sufficient to explain the observed aggregation onset, all highly aggregative isolates reproducibly reached a plateau in MP removal, with residual suspended MP concentrations typically remaining between 10^{6} and 10^{7} MPs mL^{-1} after 24 h. This decoupling between rapid encounter kinetics and incomplete MP removal indicates that productive aggregation is constrained not simply by collision frequency, but by the ability of particle encounters to generate aggregates that ultimately sediment from the water column. Because the assays were performed under continuous rolling incubation, aggregate restructuring and breakup may occur simultaneously with aggregate formation. Consequently, the observed plateau may reflect not only progressive depletion of freely suspended particles but also the establishment of a dynamic aggregation-fragmentation balance within the system.

This interpretation is further supported by the bacterial dose-response experiments (**Figure 2B**), where increasing cell abundance beyond the standard inoculum concentration did not produce proportional improvements in MP removal. If encounter frequency alone governed aggregation efficiency, higher

bacterial concentrations would be expected to consistently enhance MP capture. Instead, the observed non-linear response suggests that aggregate architecture, attachment efficiency, and sedimentation behavior become increasingly important determinants of overall MP removal.

Classical coagulation theory distinguishes between particle encounter and successful attachment, with the latter commonly described by the collision efficiency parameter (α), which is frequently below unity in natural aquatic systems (Elimelech et al., 1995; Gregory, 2006). Reduced attachment efficiencies arise from multiple physicochemical constraints, including electrostatic repulsion, hydration forces, steric hindrance, and particle surface heterogeneity. In heteroaggregation systems involving distinct particle types, such as MPs and bacterial cells, these interactions become particularly complex and strongly context-dependent (Praetorius et al., 2020).

EPS-mediated aggregation further contributes to this complexity. In marine systems, EPS and TEP promote particle adhesion while simultaneously generating highly hydrated, porous, and fractal aggregate architectures (Passow, 2002; Quigg et al., 2021). These structures increase effective particle capture but do not necessarily produce compact or rapidly sedimenting aggregates. Coagulation-based studies of marine snow formation have shown that polymer-mediated aggregation strongly influences aggregate size, porosity, and settling behavior (Mari and Burd, 1998). Importantly, TEP-rich systems often exhibit substantially higher attachment probabilities than most non-polymeric particles, highlighting the contribution of extracellular polymers to aggregate formation and stability (Passow, 2002).

Recent work examining microbial-associated MPs in natural waters further supports this interpretation by demonstrating that microbial colonization can substantially alter aggregate geometry, fractal structure, and settling velocity without necessarily enhancing net sedimentation efficiency (Nguyen et al., 2020). In particular, microbial colonization has been shown to generate larger but more porous and less compact MP-containing aggregates, thereby prolonging particle residence time in suspension despite active aggregation processes. Similar behavior has also been observed for biofilm-coated MPs interacting with biogenic particles, where aggregation efficiency and vertical transport become partially decoupled (Michels et al., 2018).

Consistent with these models, the initial reduction in suspended MPs observed in our system likely reflects rapid formation of EPS-mediated aggregates following particle contact. However, the persistence of a residual suspended fraction suggests that a proportion of particle encounters fail to generate stable attachment or produce aggregates with limited sedimentation capacity.

The transition from rapid initial aggregation to a slower approach toward a plateau is also in agreement with classical coagulation kinetics. As aggregation proceeds, both MPs and bacterial cells become progressively depleted from suspension, reducing collision frequencies and slowing subsequent aggregation rates. This depletion-driven behavior is a characteristic feature of coagulation systems and contributes to self-limiting aggregation dynamics in aquatic particle assemblages (Burd and Jackson, 2009).

Although the present data do not allow direct estimation of collision efficiency, the broadly similar timescales predicted by encounter-rate calculations and observed aggregation dynamics suggest that attachment efficiencies are unlikely to be extremely low. This interpretation is consistent with EPS-mediated aggregation processes, where extracellular polymers can substantially enhance particle stickiness and promote aggregate formation (Passow, 2002).

Together, these processes provide a mechanistic explanation for the incomplete removal of MPs observed across highly aggregative isolates. Rather than reflecting exhaustion of aggregation capacity, this plateau likely emerges from the interplay between encounter-driven aggregation, formation of porous EPS-mediated aggregates, altered sedimentation dynamics, aggregate restructuring and potential breakup under rolling conditions, and progressive depletion of freely suspended particles.

Finally, the moderate aggregation efficiencies observed under the low-ionic-strength conditions used here are consistent with systems in which electrostatic interactions are only partially screened and aggregation is likely dominated by hydrophobic interactions and polymer-mediated bridging. Under higher salinity conditions, enhanced electrostatic screening typically increases collision efficiency and promotes formation of larger and more compact aggregates, thereby facilitating particle incorporation and sedimentation (Elimelech et al., 1995; Passow, 2002).

4. MP aggregation reduces trophic transfer to aquatic grazers

To evaluate whether bacteria-mediated aggregation influences the trophic transfer of MPs, uptake assays were performed using two bacterivorous aquatic consumers with distinct feeding strategies: the environmental amoeba isolate *Acanthamoeba* sp. H13, which internalize particles through phagocytosis, and the rotifer *Brachionus plicatilis*, which feed by filtration of suspended particles. Based on the aggregation phenotypes described above, three bacterial backgrounds were selected for these experiments: the highly aggregative environmental isolate A16, the previously characterized aggregative strain *P. aeruginosa* PAO1, and the Δ*psl*

mutant, deficient in the production of the Psl exopolysaccharide previously associated with MP aggregation in PAO1.

Amoeba assays

The main results obtained with amoebae are summarized in **Figure 3**. Monitoring of suspended MPs over time (**Figure 3A**) confirmed the aggregation phenotypes previously observed in the absence of grazers. Samples containing A16 or PAO1 showed a rapid decrease in suspended MPs during the first 24 h of incubation, in agreement with efficient formation of MP-bacteria aggregates. In contrast, the PAO1 Δ*psl* mutant produced only a limited reduction in suspended MPs, with values approaching those of abiotic controls containing MPs alone. Importantly, the addition of amoebae did not substantially alter the overall kinetics of MP removal from suspension, as comparable profiles were observed in the presence and absence of amoebae for each bacterial background. These results indicate that, under these conditions, aggregation dynamics are largely controlled by bacteria rather than by grazing activity.

Microscopic examination of the samples (**Figure 3B**) revealed strong heterogeneity in MP incorporation among individual amoebae. Within all treatments, cells ranged from amoebae lacking detectable MPs to heavily loaded cells containing large intracellular accumulations of fluorescent particles. Although no absolute exclusion of MP uptake was observed in any condition, amoebae incubated with highly aggregative strains generally appeared to contain fewer MPs than those exposed to the Δ*psl* mutant. Notably, samples containing A16 consistently displayed lower amoeba densities than those incubated with PAO1 or Δ*psl*. Fluorescent MPs were observed within amoebal vacuoles, supporting particle internalization rather than exclusive surface association.

This result is consistent with the feeding mode of amoebae, which internalize particles by phagocytosis and can engulf a broad range of particle sizes, including bacteria, yeast, colloids, and synthetic microspheres (Rillig and Bonkowski, 2018). In such systems, aggregation may reduce the fraction of particles encountered per unit time but does not create a strict size exclusion barrier.

Flow cytometry analysis supported microscopy observations. Samples containing A16 exhibited significantly fewer amoeba events than PAO1 or Δ*psl* treatments (**Supplementary Figure S3**), suggesting inhibition of amoeba proliferation or survival by this isolate. To determine whether this effect was independent of MP exposure, an additional assay was performed using amoeba incubated with each bacterial strain in the absence of MPs. Whereas amoeba abundance increased from the initial inoculum to approximately 15-18 events μL^{-1} after 48 h in the presence of PAO1 or Δ*psl*, amoebae incubated with A16 remained close to the initial abundance (~2 events μL^{-1}). These findings indicate that A16 may interfere

with amoeba growth independently of MP aggregation. Importantly, because PAO1 produced a similar aggregation phenotype without affecting amoeba population expansion, the effects of bacterial aggregation on MP accessibility cannot be explained solely by the apparent anti-amoebal activity of A16.

Analysis of MP-positive amoebae further indicated that bacterial aggregation altered MP accessibility to amoebae (**Figure 3C**). Samples incubated with the poorly aggregative Δ*psl* mutant displayed significantly higher percentages of MP-positive amoebae than PAO1 samples (mean values of 81.6% and 62%, respectively), while A16 produced values comparable to PAO1 (~62%). Comparable alterations in amoeba-bacteria system dynamics have been reported under MP exposure, highlighting the sensitivity of amoeba-bacteria interactions to such perturbations (Zhou et al., 2024). These results support the idea that efficient bacterial aggregation reduces MP availability for amoebal uptake, although it does not completely prevent incorporation. Because large aggregates were removed prior to flow-cytometric analysis, amoebae associated with oversized MP-bacteria aggregates may be underrepresented in the analyzed fraction. Consequently, the reported frequencies of MP-positive amoebae should be interpreted as estimates of particle accessibility within the analyzed population rather than absolute uptake frequencies. Nevertheless, microscopy observations revealed fluorescent MPs within amoebal vacuoles across treatments, supporting the occurrence of particle internalization despite potential losses associated with the filtration step. In contrast, fluorescence intensity among MP-positive amoebae showed no significant differences between treatments (**Figure 3D**), suggesting that aggregation primarily affects the probability of particle uptake rather than intracellular particle accumulation once ingestion occurs. Mean/median fluorescence values were $2.4 \times 10^5/1.8 \times 10^5$ for Δ*psl*, $3.3 \times 10^5/2.2 \times 10^5$ for PAO1, and $3.7 \times 10^5/2.3 \times 10^5$ for A16.

Rotifer assays

The impact of bacterial aggregation on MP incorporation by rotifers is summarized in **Figure 4**. In contrast to amoebae, rotifers showed a stronger dependence on bacterial aggregation state. In control and Δ*psl* samples, addition of rotifers caused a reduction in suspended MPs relative to corresponding treatments lacking rotifers (**Figure 4A**). This effect was already visible after 3 h of incubation and became more pronounced after 24 h, indicating active uptake of dispersed particles.

By comparison, samples containing A16 or PAO1 already exhibited strongly reduced concentrations of suspended MPs prior to rotifer feeding due to the formation of large MP-bacteria aggregates maintained in suspension by roller mixing. Under these conditions, addition of rotifers produced little or no additional

decrease in suspended MPs. These observations suggest that aggregation reduced the accessibility of MPs to rotifer feeding. Large aggregates likely exceeded the optimal size range or physical configuration efficiently captured by the rotifer feeding apparatus. It should also be noted that these experiments were performed in seawater. Elevated ionic strength is known to enhance aggregation by increasing electrostatic screening and reducing repulsive interactions between particles, thereby favoring the formation of larger and more stable aggregates. Consequently, the strong reduction in rotifer-associated MPs observed here likely reflects the combined effects of bacterial EPS-mediated aggregation and physicochemical conditions that promote particle aggregation under saline conditions.

This strong dependence on aggregation state is consistent with the feeding mechanism of rotifers, which filter particles within a defined size range. Aggregation alters the effective particle size distribution, thereby influencing ingestion efficiency. Previous studies have shown that aggregation can either enhance or reduce MP ingestion depending on the resulting aggregate size. In particular, aggregated particles that fall within the feeding spectrum are ingested efficiently, whereas larger aggregates exceed the capture capacity of rotifers (Drago et al., 2020).

Accordingly, quantification of MPs retained within filtered rotifers (**Figure 4B**) revealed significantly higher MP loads in control and Δ*psl* treatments than in A16 or PAO1 samples. Mean values reached 3.6×10^3 and 2.4×10^3 MPs per rotifer in control and Δ*psl* samples, respectively, compared with approximately 1×10^3 and 9×10^2 MPs in A16 and PAO1 treatments. Microscopy observations further supported these results, as rotifers from control and Δ*psl* groups displayed visibly higher intracellular fluorescence and MP accumulation than those exposed to highly aggregative bacterial backgrounds (**Figure 4C**). Fluorescent MPs were clearly visible within the digestive tract of rotifers, supporting ingestion rather than simple external attachment of particles.

More broadly, ingestion of MPs by zooplankton is known to depend strongly on particle properties, including size, shape, and physicochemical signals, as well as on species-specific feeding strategies (Botterell et al., 2020). Thus, aggregation represents a key process modifying these parameters and, consequently, trophic transfer. In addition, rotifers and other zooplankton can exhibit selective feeding and rejection behaviors, have been suggested to re-ingest or recycle MPs under certain conditions, further complicating MP dynamics at the base of food webs (Bermúdez et al., 2025).

Collectively, these results indicate that bacteria-mediated aggregation can strongly alter MP trophic transfer, although the magnitude of this effect depends on grazer feeding strategy. While aggregation produced only a moderate reduction

in MP uptake by amoebae, it dramatically reduced MP availability for trophic transfer to rotifers, highlighting the importance of feeding mode in determining the ecological consequences of MP sequestration.

Such variability is consistent with broader observations of MP trophic transfer, which show that ingestion occurs across many taxa but is highly heterogeneous and often limited by particle characteristics and environmental context (Gouin, 2020). Aggregation therefore acts as a key regulator of MP bioavailability at the base of aquatic food webs.

Importantly, these observations should not be generalized to all aquatic consumers, as feeding selectivity varies substantially among taxa. The amoebae and rotifers used here behave largely as opportunistic non-selective bacterivorous grazers, whereas other organisms such as copepods display active prey selection based on particle size, morphology, motility, and chemical composition. Likewise, filter-feeding mollusks may respond differently to bacteria-mediated aggregation depending on aggregate size, compactness, and settling behavior. Thus, bacterial aggregation may not universally reduce MP uptake across aquatic food webs, but instead redistribute MPs among trophic pathways by modifying their physicochemical presentation and bioavailability to different consumers.

5. Engineering of a highly aggregative isolate for PET surface modification

Because efficient polymer transformation in aquatic environments requires sustained physical association between microbial cells and particle surfaces, we next explored whether highly MP-aggregative bacteria could be repurposed as chassis for targeted plastic surface modification. Based on its strong aggregation phenotype, robust performance under different hydrodynamic conditions, and predicted capacity for efficient particle association, the environmental isolate A16 was engineered to express FastPETase, a PET hydrolase previously shown to enhance PET deconstruction relative to earlier PETase variants (Lu et al., 2022). To contextualize the performance of A16, a parallel construct was generated in PAO1 as a genetically tractable laboratory strain widely used for heterologous expression studies.

PET films were incubated with the different bacterial strains and subsequently subjected to a stringent post-incubation cleaning protocol prior to FTIR analysis, minimizing contributions from loosely associated biomass and extracellular material. Targeted analysis of the diagnostic PET bands at 1340 and 1370 cm^{-1} revealed reproducible differences between FastPETase-expressing strains and their corresponding parental backgrounds (**Figure 5**). These bands are associated with distinct methylene conformations within PET and have previously been used

to evaluate changes in the relative contribution of amorphous and crystalline polymer domains (Chen et al., 2012). In particular, PET films incubated with PAO1-FastPETase showed a consistent decrease in the intensity of the 1370 cm^{-1} band relative to the 1340 cm^{-1} band, resulting in an increased 1340/1370 peak-area ratio. A similar, although less pronounced, trend was observed for A16-FastPETase.

These spectral changes indicate that expression of FastPETase is associated with detectable alterations in PET surface properties. However, the observed modifications should not be interpreted as direct evidence of polymer depolymerization. Rather, they are consistent with changes in PET surface chemistry and/or in the relative contribution of amorphous and crystalline domains at the polymer surface. Additional approaches, such as mass-loss measurements or quantification of soluble degradation products, would be required to directly demonstrate PET hydrolysis and depolymerization.

Importantly, no evidence of polystyrene degradation by isolates A16, A20, or P5 was detected by FTIR analyses following incubation with polystyrene substrates. This observation indicates that the strong reduction of suspended MPs observed throughout the aggregation assays was driven primarily by particle aggregation and sedimentation rather than by polymer biodegradation. Together with the physical aggregation framework developed in Sections 2 and 3, these findings support a conceptual distinction between particle sequestration and polymer transformation.

Consistent with this interpretation, the rapid encounter-driven aggregation dynamics described above likely facilitate prolonged contact between bacterial cells and polymer surfaces, thereby increasing opportunities for localized enzymatic activity once particles become incorporated into EPS-rich aggregates. In natural aquatic systems, where hydrodynamic constraints limit encounter rates, such physical association has been recognized as a key determinant of biofilm-mediated surface processes (Fulaz et al., 2019).

Despite the limitations inherent to FTIR-based analyses, the results demonstrate that the highly aggregative isolate A16 can be functionally engineered to generate detectable modifications in PET surface spectral properties. Notably, this engineered functionality was implemented in a strain originally selected for its ability to aggregate and sequester polystyrene MPs from suspension.

Collectively, these findings suggest that strong MP-aggregating bacteria may serve as modular platforms for plastic-interacting functions, coupling efficient particle capture with engineered catalytic activities. Rather than functioning solely as passive aggregators, such strains could potentially act as delivery chassis that increase the residence time of plastic-associated enzymes at polymer surfaces under environmentally realistic conditions, where sustained particle association is

likely essential for effective enzymatic activity. Future work combining complementary analytical approaches, including mass-loss measurements and soluble product quantification, will be necessary to determine the extent of polymer depolymerization achieved by these engineered systems.

Data availability

The raw sequencing data generated in this study have been deposited in the NCBI BioProject database under the accession number PRJNA1467704.

References

1. Wang, X., Bolan, N., Tsang, D.C.W., Sarkar, B., Bradney, L. & Li, Y. (2021). A review of microplastics aggregation in aquatic environment: Influence factors, analytical methods, and environmental implications. Journal of Hazardous Materials 402, 123496.
2. Zhang, X., Chen, X., Liu, Z., Pan, X., Zheng, X., Li, Y., Liao, X. & Wang, J. (2024). Microbial colonization of microplastic in aquatic environments: Toxicity, degradation potential and interactions. TrAC Trends in Analytical Chemistry 181, 118028.
3. Botterell, Z.L.R., Beaumont, N., Cole, M., Hopkins, F.E., Steinke, M., Thompson, R.C. & Lindeque, P.K. (2020). Bioavailability of microplastics to marine zooplankton: Effect of shape and infochemicals. Environmental Science & Technology 54(19), 12024–12033.
4. Gouin, T. (2020). Toward an improved understanding of the ingestion and trophic transfer of microplastic particles: Critical review and implications for future research. Environmental Toxicology and Chemistry 39(6), 1119–1137.
5. Zettler, E.R., Mincer, T.J. & Amaral-Zettler, L.A. (2013). Life in the “plastisphere”: Microbial communities on plastic marine debris. Environmental Science & Technology 47(13), 7137–7146.
6. Bryant, J.A., Clemente, T.M., Viviani, D.A., Fong, A.A., Thomas, K.A., Karl, D.M., White, A.E. & DeLong, E.F. (2016). Diversity and activity of communities inhabiting plastic debris in the North Pacific Gyre. mSystems 1(3), e00024–16.
7. Miao, L., Wang, P., Hou, J., Yao, Y., Liu, Z., Liu, S. & Li, T. (2021). Distinct community structure and microbial functions of plastisphere in freshwater

ecosystems revealed by high-throughput sequencing. Environmental Pollution 268, 118123.

8. Wright, R.J., Erni-Cassola, G., Zadjelovic, V., Latva, M. & Christie-Oleza, J.A. (2020). Marine plastic debris: A new surface for microbial colonization. Frontiers in Environmental Science 8, 574274.

9. Song, H., Xiao, S., Zhou, X., Li, Y., Tao, M., Wu, F. & Xu, X. (2024). Temporal dynamics of bacterial colonization on five types of microplastics in a freshwater lake. Science of the Total Environment 913, 169697.

10. Cholewińska, P., Wojnarowski, K., Moniuszko, H., Pokorny, P. & Palić, D. (2025). An exploratory review of microplastic pollution, associated microbiomes and pathogens in water. Applied Sciences 15(15), 8128.

11. Long, M., Moriceau, B., Gallinari, M., Lambert, C., Huvet, A., Raffray, J. & Soudant, P. (2015). Interactions between microplastics and phytoplankton aggregates: Impact on their respective fates. Marine Chemistry 175, 39–46.

12. Kooi, M., van Nes, E.H., Scheffer, M. & Koelmans, A.A. (2017). Ups and downs in the ocean: Effects of biofouling on vertical transport of microplastics. Environmental Science & Technology 51(14), 7963–7971.

13. Passow, U. (2002). Transparent exopolymer particles (TEP) in aquatic environments. Progress in Oceanography 55, 287–333.

14. Burd, A.B. & Jackson, G.A. (2009). Particle aggregation. Annual Review of Marine Science 1, 65–90.

15. Quigg, A., Santschi, P.H., Burd, A., Chin, W.C., Kamalanathan, M., Xu, C. & Ziervogel, K. (2021). From nano-gels to marine snow: A synthesis of gel formation processes and modeling efforts involved with particle flux in the ocean. Gels 7, 114.

16. Michels, J., Stippkugel, A., Lenz, M., Wirtz, K. & Engel, A. (2018). Rapid aggregation of biofilm-covered microplastics with marine biogenic particles. Proceedings of the Royal Society B 285, 20181203.

17. Nguyen, T.H., Tang, F.H.M. & Maggi, F. (2020). Sinking of microbial-associated microplastics in natural waters. PLoS ONE 15(2), e0228209.

18. Romero, M., Carabelli, A., Swift, M.R. & Smith, M.I. (2022). Fluid dynamics and cell-bound Psl polysaccharide allows microplastic capture, aggregation and subsequent sedimentation by Pseudomonas aeruginosa in water. Environmental Microbiology 24(3), 1560–1572.

19. Weisburg, W. G., Barns, S. M., Pelletier, D. A., & Lane, D. J. (1991). 16S ribosomal DNA amplification for phylogenetic study. Journal of bacteriology 173(2), 697–703.

20. Daugberg, A.O.H., Waldisperg, A., Riisgaard-Jensen, M., Vestergaard, S.Z., Sánchez Navarro, R., Weber, T., Blin, K., Shaw, S., Nielsen, P.H. & Dueholm, M.K.D. (2025). epsSMASH uncovers exopolysaccharide biosynthetic gene clusters in environmental and human microbiomes. bioRxiv. https://doi.org/10.64898/2025.12.21.693542.

21. van den Belt, M., Gilchrist, C., Booth, T.J., Chooi, Y.H., Medema, M.H. & Alanjary, M. (2023). CAGECAT: The comparative gene cluster analysis toolbox for rapid search and visualisation of homologous gene clusters. BMC Bioinformatics 24, 181.

22. Lu, H., Diaz, D.J., Czarnecki, N.J., Zhu, C., Kim, W., Shroff, R., Acosta, D.J., Alexander, B.R., Cole, H.O., Zhang, Y., Lynd, N.A., Ellington, A. D. & Alper, H.S. (2022). Machine learning-aided engineering of hydrolases for PET depolymerization. Nature 604, 662–667.

23. Kim, H. R., Lee, H. M., Yu, H. C., Jeon, E., Lee, S., Li, J., & Kim, D. H. (2020). Biodegradation of polystyrene by Pseudomonas sp. isolated from the gut of superworms (larvae of Zophobas atratus). Environmental science & technology 54(11), 6987-6996.

24. Miravalle, E., Balboa, S., Zanetti, M., Otero, A., & Lazzari, M. (2024). New insights on the degradation of polystyrene and polypropylene by larvae of the superworm Zophobas atratus and gut bacterial consortium enrichments obtained under different culture conditions. Journal of Hazardous Materials 478, 135475.

25. Chen, Z., Hay, J.N., & Jenkins, M.J. (2012). FTIR spectroscopic analysis of poly(ethylene terephthalate) on crystallization. European Polymer Journal, 48(9), 1586-1610.

26. Islam, S.T. & Lam, J.S. (2014). Synthesis of bacterial polysaccharides via the Wzx/Wzy-dependent pathway. Canadian Journal of Microbiology 60(11), 697–716.

27. Kiørboe, T. (2003). Marine snow microbial communities: Scaling of abundances with aggregate size. Aquatic Microbial Ecology 33, 67–75.

28. Smoluchowski, M. (1917). Versuch einer mathematischen Theorie der Koagulationskinetik kolloider Lösungen. Zeitschrift für physikalische Chemie 92, 129–168.

29. Elimelech, M., Gregory, J., Jia, X. & Williams, R.A. (1995). Particle deposition and aggregation: Measurement, modelling, and simulation. Butterworth-Heinemann.

30. Gregory, J. (2006). Particles in water: Properties and processes. CRC Press.

31. Praetorius, A., et al. (2020). Strategies for determining heteroaggregation attachment efficiencies of engineered nanoparticles in aquatic environments. Environmental Science: Nano 7, 351–367.

32. Mari, X. & Burd, A. (1998). Seasonal size spectra of transparent exopolymeric particles (TEP) in a coastal sea. Marine Ecology Progress Series 163, 63–76.

33. Rillig, M.C. & Bonkowski, M. (2018). Microplastic and soil protists: A call for research. Environmental Pollution 241, 1128–1131.

34. Zhou, M., Ma, L., Wang, Z., Li, S., Cai, Y., Li, M., Zhang, L., Wang, C., Wu, B., Yan, Q., He, Z. & Shu, L. (2024). Nano- and microplastics drive the dynamic equilibrium of amoeba-associated bacteria and antibiotic resistance genes. Journal of Hazardous Materials 476, 134958.

35. Drago, C., Pawlak, J. & Weithoff, G. (2020). Biogenic aggregation of small microplastics alters their ingestion by a common freshwater micro-invertebrate. Frontiers in Environmental Science 8, 574274.

36. Bermúdez, J.R., Jolo, R., Swarzenski, P.W., Oberhänsli, F., Taylor, A., Alonso, C., Metian, M. & Nejstgaard, J.C. (2025). A marine plankton–plastic predation loop: Selective grazing, excretion and reingestion of microplastics by the rotifer Brachionus plicatilis. Microplastics and Nanoplastics 5, 40.

37. Fulaz, S., Vitale, S., Quinn, L., & Casey, E. (2019). Nanoparticle-Biofilm Interactions: The Role of the EPS Matrix. Trends in microbiology, 27(11), 915–926.

Acknowledgements

This work was supported by Grant CNS2023-145299 funded by MICIU/AEI/10.13039/501100011033 and by the European Union NextGenerationEU/PRTR. Sergio Silva-Bea was supported by the Spanish Ministry of Universities through a Formación de Profesorado Universitario (FPU) fellowship (FPU21/01147).

Contributions

1. M.R.: Conceptualization, supervision, data interpretation, writing - original draft and review & editing.
2. J.R.L.: Investigation, data curation, formal analysis, writing - original draft.
3. A.O.: Conceptualization, supervision, review & editing.
4. J.J.N.F., S.S.B., and J.L.: Investigation and formal analysis (amoeba flow-cytometry experiments).
5. M.T.: Formal analysis and data interpretation (FTIR analyses).
6. All authors reviewed and approved the final manuscript.

Figures and tables

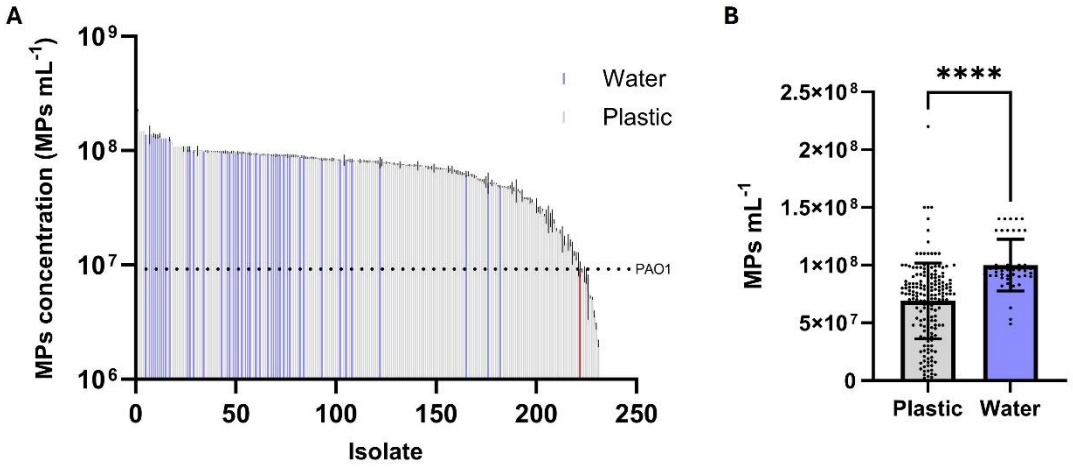


Figure 1. Environmental isolates recovered from plastic debris are enriched in MP aggregation phenotypes. (A) Screening of 230 bacterial isolates recovered from plastic debris and surrounding water samples from the Sar River for their ability to reduce suspended polystyrene MPs after 24 h under rolling incubation. Isolates are ranked according to increasing MP aggregation activity (i.e. decreasing MP concentration). Gray bars represent plastic-associated isolates, blue bars represent isolates recovered from surrounding water samples, and the red bar indicates the reference strain *Pseudomonas aeruginosa* PAO1. The dotted line indicates the mean MP concentration obtained with the reference strain PAO1. **(B)** Comparison of MP concentrations remaining in suspension after incubation with isolates recovered from plastic debris and surrounding water samples. Plastic-associated isolates showed significantly greater MP aggregation capacity than water-derived isolates. Data represent mean ± SD (n = 184 plastic isolates, n = 46 water isolates). Statistical significance was determined using the Mann-Whitney test (****$p < 0.0001$).

Table 1. High-performing MP-aggregating isolates identified during screening. Identification and aggregation phenotypes of environmental isolates displaying MP removal comparable to or greater than the reference strain *Pseudomonas aeruginosa* PAO1 after 24 h of rolling incubation. Residual MP concentrations (Values represent mean ± SD from n = 3 independent experiments) and corresponding percentage reductions relative to a no-bacteria control are shown. Isolates tentatively identified based on 16S rRNA sequencing are indicated in parentheses, whereas those confirmed by whole-genome sequencing are shown with full species names. Corresponding type strains used for comparative analyses are included.

Isolate/ strain	Identification	Sample type	Residual MP concentration (MPs mL^{-1}, mean± SD)	Reduction relative to no-bacteria control (%)
A16	*Pseudomonas parakoreensis*	Plastic-associated	$2.1 \times 10^6 \pm 1.4 \times 10^5$	97.9
P5	*Deinococcus aquaticus*	Plastic-associated	$2.9 \times 10^6 \pm 1.9 \times 10^5$	97.1
A25	*Pseudomonas* sp. *(P. koreensis)*	Plastic-associated	$5.1 \times 10^6 \pm 1.9 \times 10^5$	94.9
L4	*Pseudomonas* sp. *(P. lurida)*	Plastic-associated	$5.2 \times 10^6 \pm 1.4 \times 10^5$	94.8
A20	*Acinetobacter johnsonii*	Plastic-associated	$5.8 \times 10^6 \pm 2.5 \times 10^6$	94.2
A2	*Acinetobacter wuhuoensis*	Plastic-associated	$6.1 \times 10^6 \pm 2.7 \times 10^6$	93.9
P3	*Pseudomonas* sp. *(P. simiae)*	Plastic-associated	$8.0 \times 10^6 \pm 1.2 \times 10^6$	92.0
D6	*Pseudomonas* sp. *(P. solani)*	Plastic-associated	$8.4 \times 10^6 \pm 1.3 \times 10^6$	91.6
D3	*Bacillus* sp. *(B. wiedmannii)*	Plastic-associated	$9.0 \times 10^6 \pm 3.5 \times 10^5$	91.0
PAO1	*Pseudomonas aeruginosa*	Reference strain	$9.2 \times 10^6 \pm 1.4 \times 10^6$	90.8
K8	*Bacillus mycoides*	Plastic-associated	$1.0 \times 10^7 \pm 2.4 \times 10^6$	89.6
A12	*Acidovorax* sp. *(A. caeni)*	Plastic-associated	$1.2 \times 10^7 \pm 1.0 \times 10^6$	88.0
L17	*Pantoea sp. (P. rodasii)*	Plastic-associated	$1.3 \times 10^7 \pm 8.7 \times 10^5$	87.4
A13	*Stenotrophomonas nematodicola*	Plastic-associated	$1.3 \times 10^7 \pm 2.9 \times 10^6$	87.1
LMG 32251^T	*Pseudomonas parakoreensis*	Type strain	$8.7 \times 10^7 \pm 2.2 \times 10^6$	13.0
DSM 18376^T	*Deinococcus aquaticus*	Type strain	$9.3 \times 10^7 \pm 3.1 \times 10^6$	7.1
DSM 6963^T	*Acinetobacter johnsonii*	Type strain	$1.0 \times 10^8 \pm 3.8 \times 10^6$	0

A

Strain	Total EPS operons	WZY operons	Other EPS operons	Comparison with reference strain	WZY-dependent structural variation
Pseudomonas parakoreensis A16	4	2	Alginate, PNAG-pga	PNAG-pga absent in reference strain	WZY-dependent rearrangement
Acinetobacter johnsonii A20	2	1	PNAG-pga	PNAG-pga absent in reference strain	WZY-dependent rearrangement
Deinococcus aquaticus P5	3	3	None detected	Expanded WZY-dependent repertoire	No close correspondence with reference WZY-dependent operon

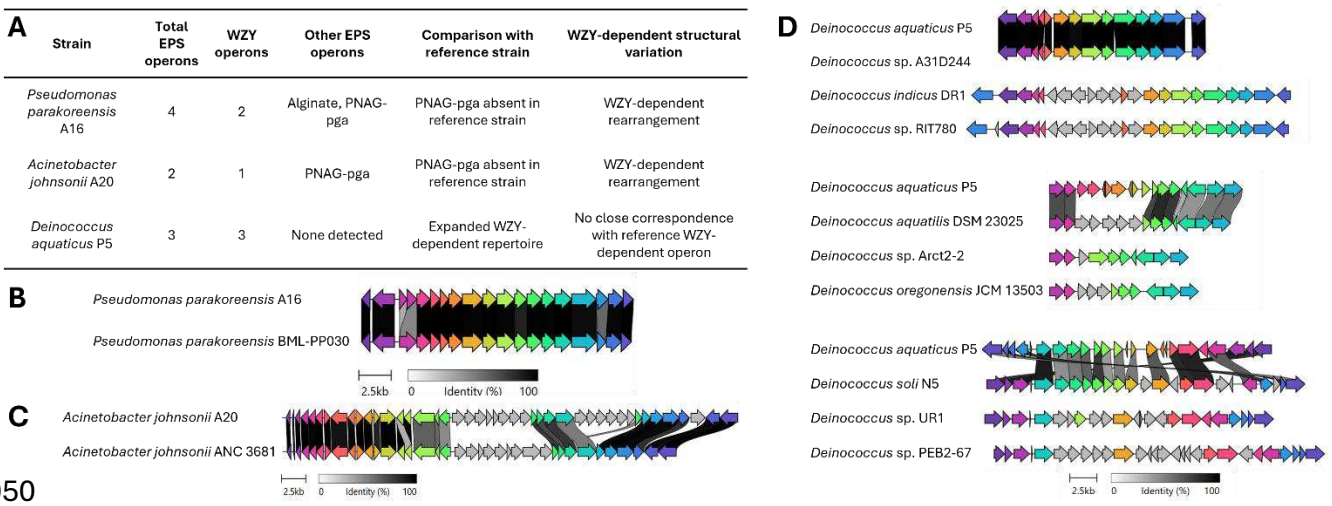
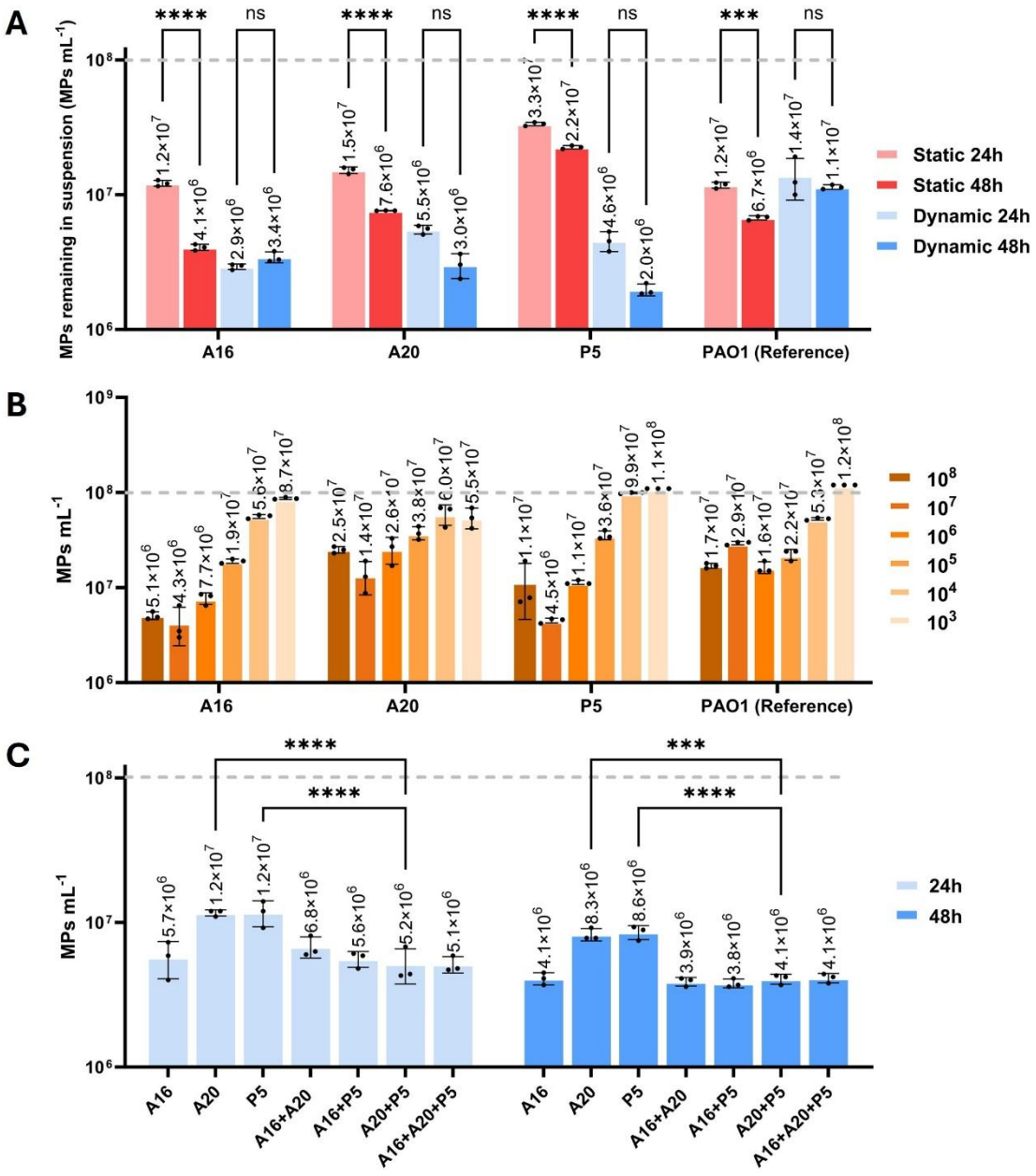


Figure S1. Diversification of EPS-associated loci in environmental MP-aggregating isolates. (A) Summary of extracellular polysaccharide (EPS) biosynthetic operons identified in the high-performing environmental isolates *Pseudomonas parakoreensis* A16, *Acinetobacter johnsonii* A20, and *Deinococcus aquaticus* P5. Total EPS operons, WZY-dependent systems, additional EPS-associated loci, and major structural differences relative to corresponding reference strains are indicated. **(B-D)** Comparative analysis of WZY-dependent EPS biosynthetic loci using CAGECAT. Conserved homologous genes are represented by matching colors. **(B)** Comparison of WZY-dependent operons in *P. parakoreensis* A16 and the reference strain BML-PP030, showing overall conservation with apparent local differences in gene organization. **(C)** Comparison of the WZY-dependent operon in *A. johnsonii* A20 and the reference strain ANC 3681, revealing extensive gene rearrangement. **(D)** Comparative analysis of the three WZY-dependent operons identified in *D. aquaticus* P5. None showed close correspondence with the operon present in the *D. aquaticus* reference strain; instead, homologous loci were distributed across multiple *Deinococcus* species, indicating diversification of EPS-associated systems within the genus.



1069

1070 **Figure 2. Aggregation dynamics of selected MP-aggregating isolates under**
1071 **different incubation conditions and bacterial concentrations. (A)** Effect of
1072 incubation regime and time on the removal of suspended MPs. Cultures were
1073 incubated under dynamic (roller mixing, 33 rpm) or static conditions for 24 or 48 h.
1074 Environmental isolates A16 (*Pseudomonas parakoreensis*), A20 (*Acinetobacter*
1075 *johnsonii*), and P5 (*Deinococcus aquaticus*) showed significantly greater
1076 reductions in suspended MPs under dynamic conditions, whereas the reference
1077 strain *Pseudomonas aeruginosa* PAO1 displayed comparatively limited sensitivity
1078 to incubation regime. **(B)** Effect of bacterial concentration on MP aggregation under
1079 dynamic incubation conditions after 24 h. Increasing bacterial concentration
1080 generally enhanced MP removal; however, aggregation efficiency approached a
1081 plateau at high cell densities, with residual suspended MP concentrations

consistently converging near ~10^6 MPs mL^{-1}. **(C)** Effect of mixed bacterial cultures on MP aggregation under dynamic incubation conditions after 24 and 48 h. Mixed cultures containing two or three environmental isolates generally did not outperform the most efficient individual isolate. An exception was observed for the A20+P5 consortium, which produced significantly enhanced MP removal compared with the corresponding monocultures. Data are presented as mean ± SD. The y-axis is shown on a logarithmic scale and represents the concentration of MPs remaining in suspension (MPs mL^{-1}). Statistical significance was determined using ordinary two-way ANOVA followed by Bonferroni's multiple comparisons test.

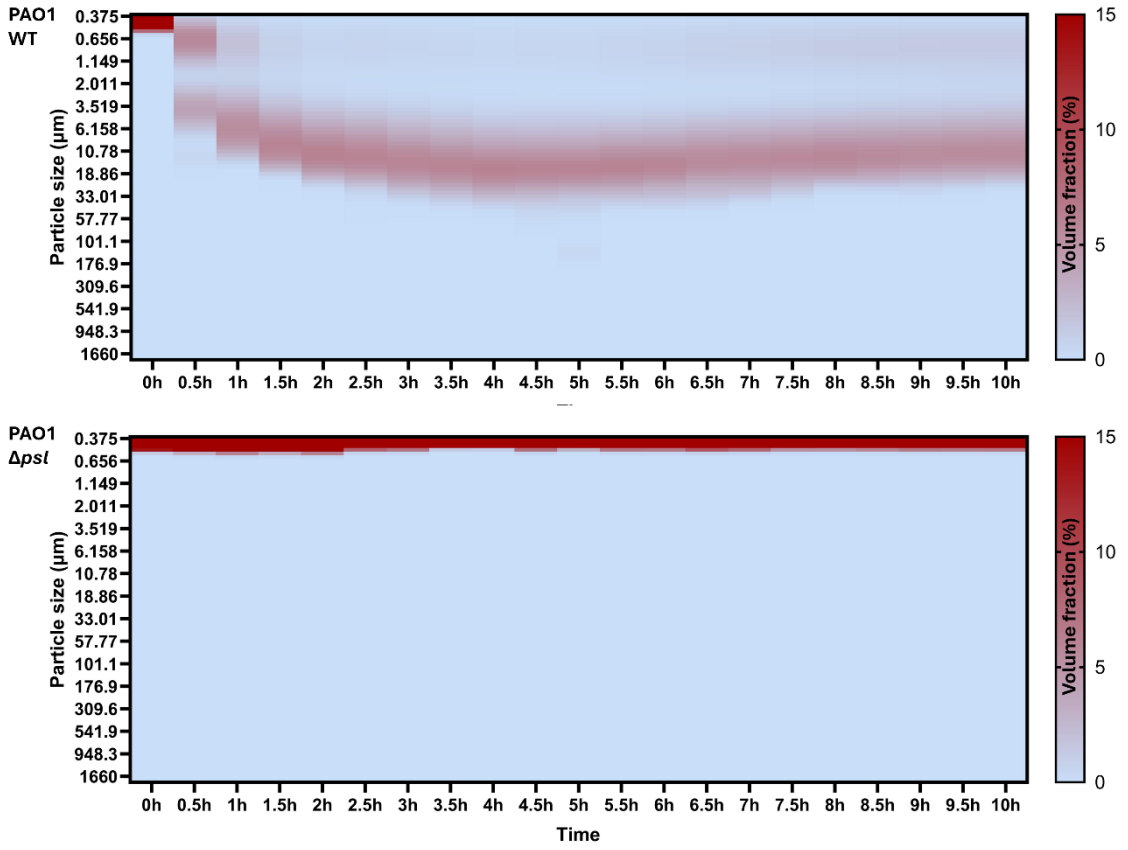


Figure S2. Temporal evolution of particle-size distributions during MP aggregation monitored by laser diffraction. Heat maps represent the relative particle volume distribution (%) across particle-size classes during aggregation assays previously reported by Romero et al. (2022). Colors indicate the percentage of total diffraction volume associated with each size class at a given time point. (A) *Pseudomonas aeruginosa* PAO1 wild type strain. (B) PAO1 Δ*psl* mutant. In PAO1, the dominant particle population progressively shifted from submicron particles to aggregates of approximately 10-20 µm within the first 3-5 h of incubation, after which only minor changes were observed. In contrast, the Δ*psl* mutant showed little redistribution of particle sizes over time, consistent with its impaired aggregation phenotype. These data illustrate the rapid kinetics of EPS-dependent aggregate formation and the subsequent transition toward a quasi-steady particle-size distribution. Particle size bins correspond to the logarithmically spaced classes generated by the laser diffraction instrument.

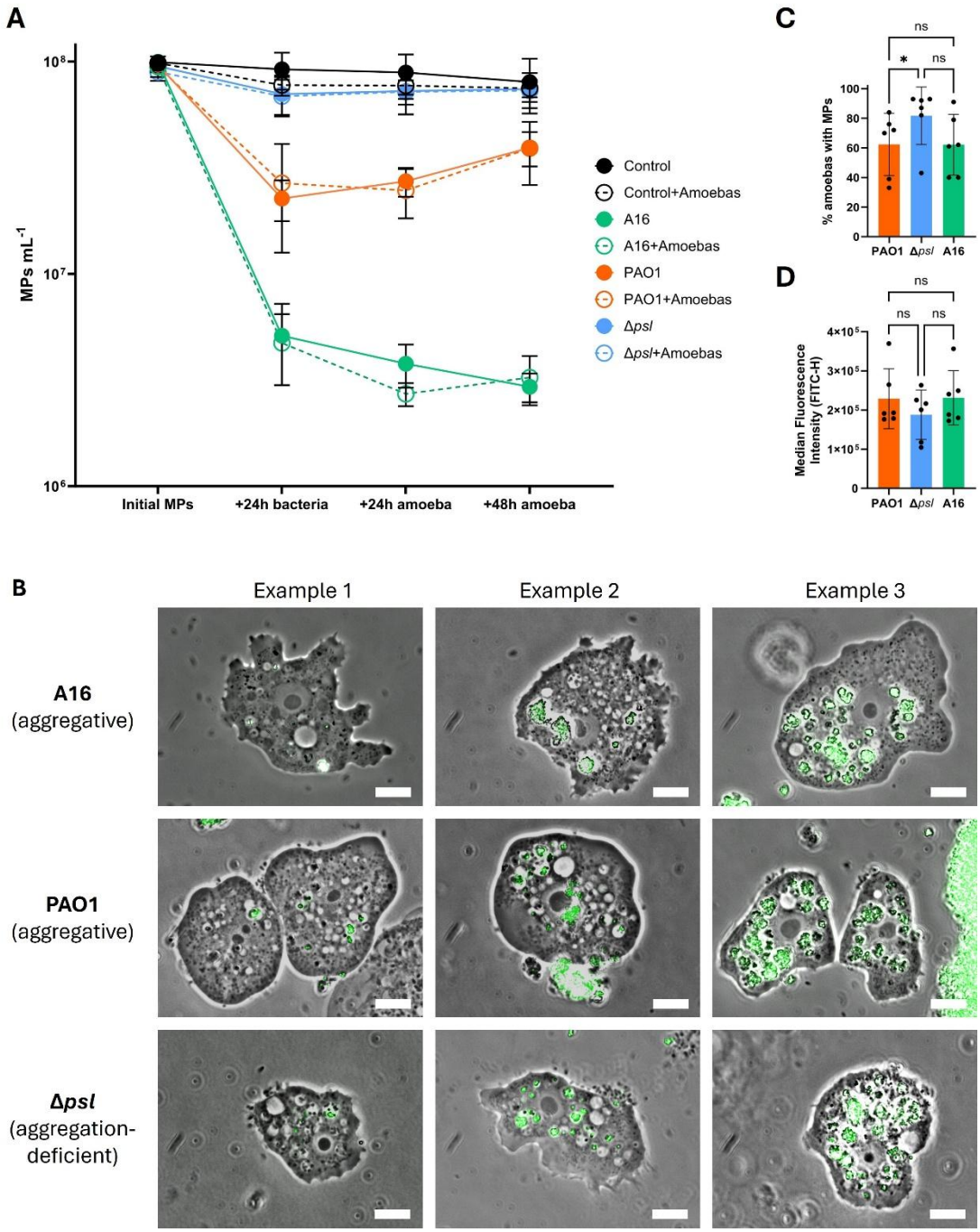


Figure 3. Highly aggregative bacteria promote MP sequestration while differentially affecting amoeba-associated particle uptake. (A) Quantification of suspended MPs throughout the sequential incubation assay. MPs were first incubated with bacterial strains for 24 h, followed by the addition of amoebae and further incubation for either 24 h or 48 h. Data are shown for control samples (without bacteria), *Pseudomonas parakoreensis* A16, *Pseudomonas aeruginosa* PAO1, and the aggregation-deficient Δ*psl* mutant, in the presence or absence of amoebae. Values represent mean ± SD. **(B)** Representative fluorescence microscopy images showing amoebae after exposure to MP aggregates formed by A16, PAO1, or the Δ*psl* mutant. Green fluorescence corresponds to internalized

fluorescent MPs. Images were acquired by combining epifluorescence microscopy with transmitted-light phase-contrast observations. Three representative amoebae are shown for each bacterial treatment to illustrate the range of observed intracellular particle accumulation. Scale bars, 10 µm. **(C)** Percentage of amoebae containing internalized fluorescent MPs after 48 h of co-incubation with preformed bacterial-MP aggregates. Individual data points represent independent biological replicates. Statistical comparisons were performed using one-way ANOVA followed by Tukey's multiple-comparison test ($p < 0.05$; ns, not significant). **(D)** Median fluorescence intensity of amoebae containing MPs, used as a proxy for the relative intracellular MP load per amoeba. Bars represent mean ± SD; individual points correspond to independent biological replicates. Statistical analysis as described for panel C.

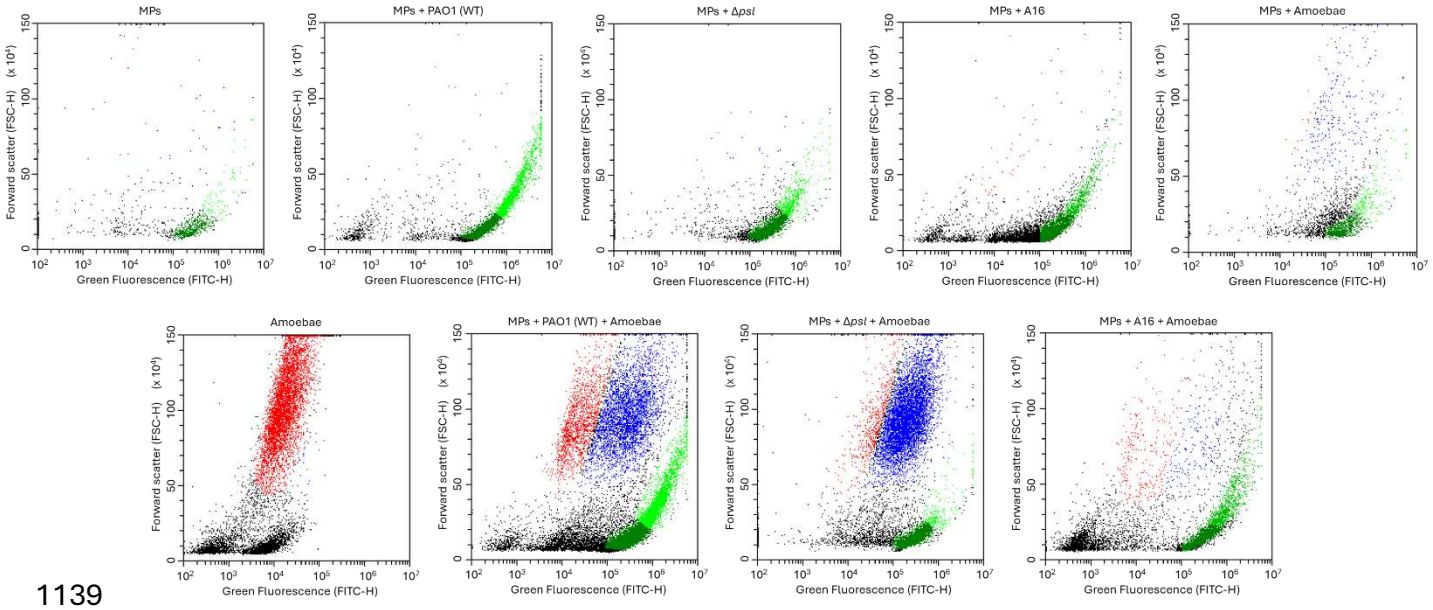
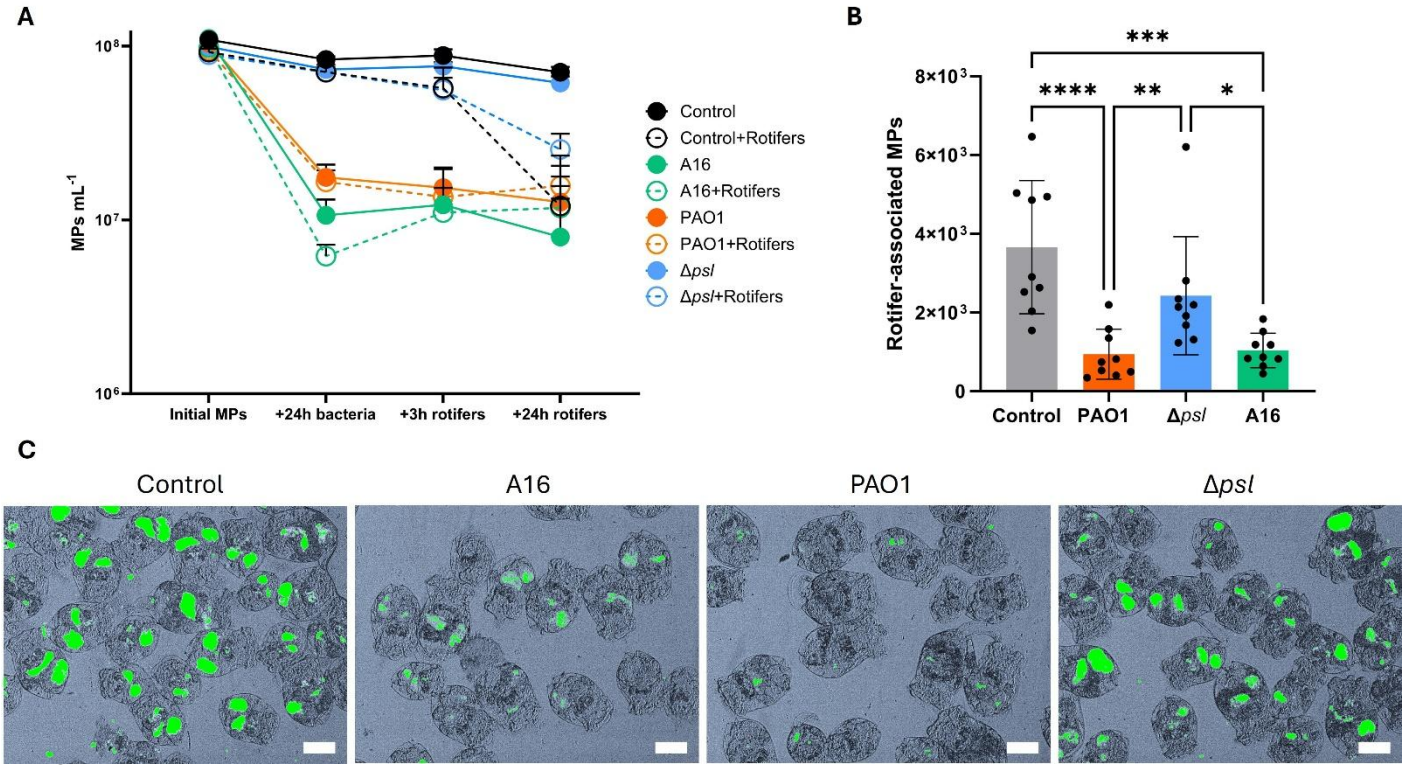


Figure S3. Representative flow cytometry gating strategy used to identify amoebae and MP-positive amoebae. Representative FSC-H versus FITC-H cytograms obtained from control samples and experimental treatments used in the amoeba uptake assays. Upper panels show control populations including fluorescent MPs alone, MPs incubated with bacterial strains, and MPs incubated with amoebae. Lower panels show amoebae alone and amoebae exposed to MPs in the presence of the indicated bacterial strains. Green events correspond to the MP gate, red events correspond to amoebae lacking detectable MP-associated fluorescence, and blue events correspond to MP-positive amoebae. Notably, the abundance of amoeba-associated events remained low in A16-containing samples, consistent with the absence of the population expansion observed in PAO1 and Δ*psl* treatments. Gates were defined using the corresponding control samples and subsequently applied to all experimental conditions. The proportion of MP-positive amoebae and fluorescence intensity values reported in Figure 3D were calculated from the gated populations shown here.



1158 **Figure 4. EPS-mediated aggregation reduces trophic transfer of MPs to rotifers.**
1159 **(A)** Quantification of suspended MPs during sequential incubation with bacterial
1160 strains and rotifers. MPs were first incubated with bacteria for 24 h before rotifers
1161 were added. Suspended MPs were quantified 3 h and 24 h after rotifer addition.
1162 Data are shown for control samples (without bacteria), *Pseudomonas*
1163 *parakoreensis* A16, *Pseudomonas aeruginosa* PAO1, and the aggregation-deficient
1164 Δ*psl* mutant, in the presence or absence of rotifers. Values represent mean ± SD.
1165 **(B)** Quantification of rotifer-associated MPs after 24 h of exposure to bacterial-MP
1166 suspensions. Individual points represent independent biological replicates. Bars
1167 indicate mean ± SD. Statistical significance was determined by one-way ANOVA
1168 followed by Tukey's multiple-comparison test ($p < 0.05$; *$p < 0.01$; **$p < 0.001$; ***p
1169 < 0.0001). **(C)** Representative microscopy images of rotifers after exposure to
1170 fluorescent MPs in the absence of bacteria (Control) or following incubation with
1171 A16, PAO1, or the Δ*psl* mutant. Images were acquired using epifluorescence
1172 microscopy combined with transmitted-light bright-field illumination, enabling
1173 simultaneous visualization of rotifers and fluorescent MPs. Fluorescent MPs are
1174 visible within the digestive tract of rotifers, supporting particle ingestion. Scale
1175 bars, 150 µm.

1176

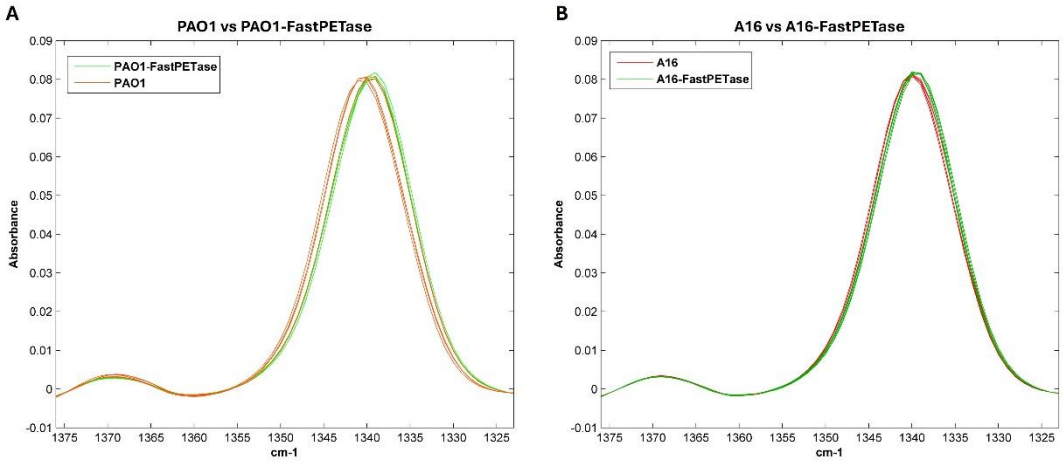


Figure 5. ATR-FTIR analysis of PET films following incubation with parental and FastPETase-expressing bacterial strains. (A) Enlarged view of the 1320-1380 cm^{-1} region of PET spectra obtained from films incubated with *Pseudomonas parakoreensis* A16 and A16-FastPETase for 18 days. PET films exposed to the FastPETase-expressing strain showed an increase in the relative intensity of the 1340 cm^{-1} band and a corresponding decrease in the 1370 cm^{-1} band, resulting in an increased 1340/1370 peak ratio. **(B)** Enlarged view of the 1320-1380 cm^{-1} region of PET spectra obtained from films incubated with *Pseudomonas aeruginosa* PAO1 and PAO1-FastPETase for 18 days. Similar spectral changes were observed, characterized by a relative increase of the 1340 cm^{-1} band and a decrease of the 1370 cm^{-1} band.

The 1340 and 1370 cm^{-1} bands have previously been associated with distinct methylene conformations within PET. Changes in the relative intensity of these bands are consistent with alterations in PET surface structure.